

Figure S1

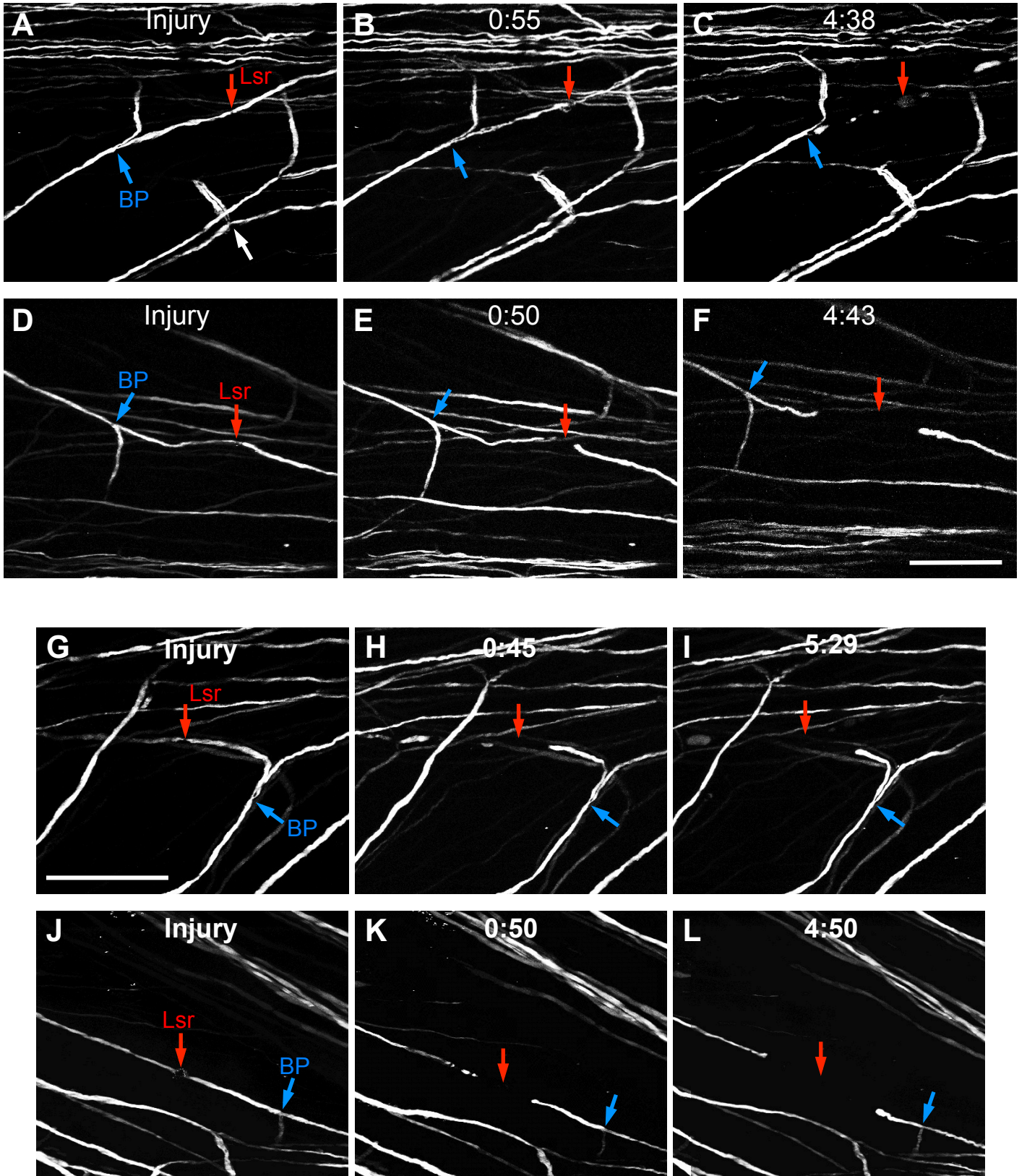
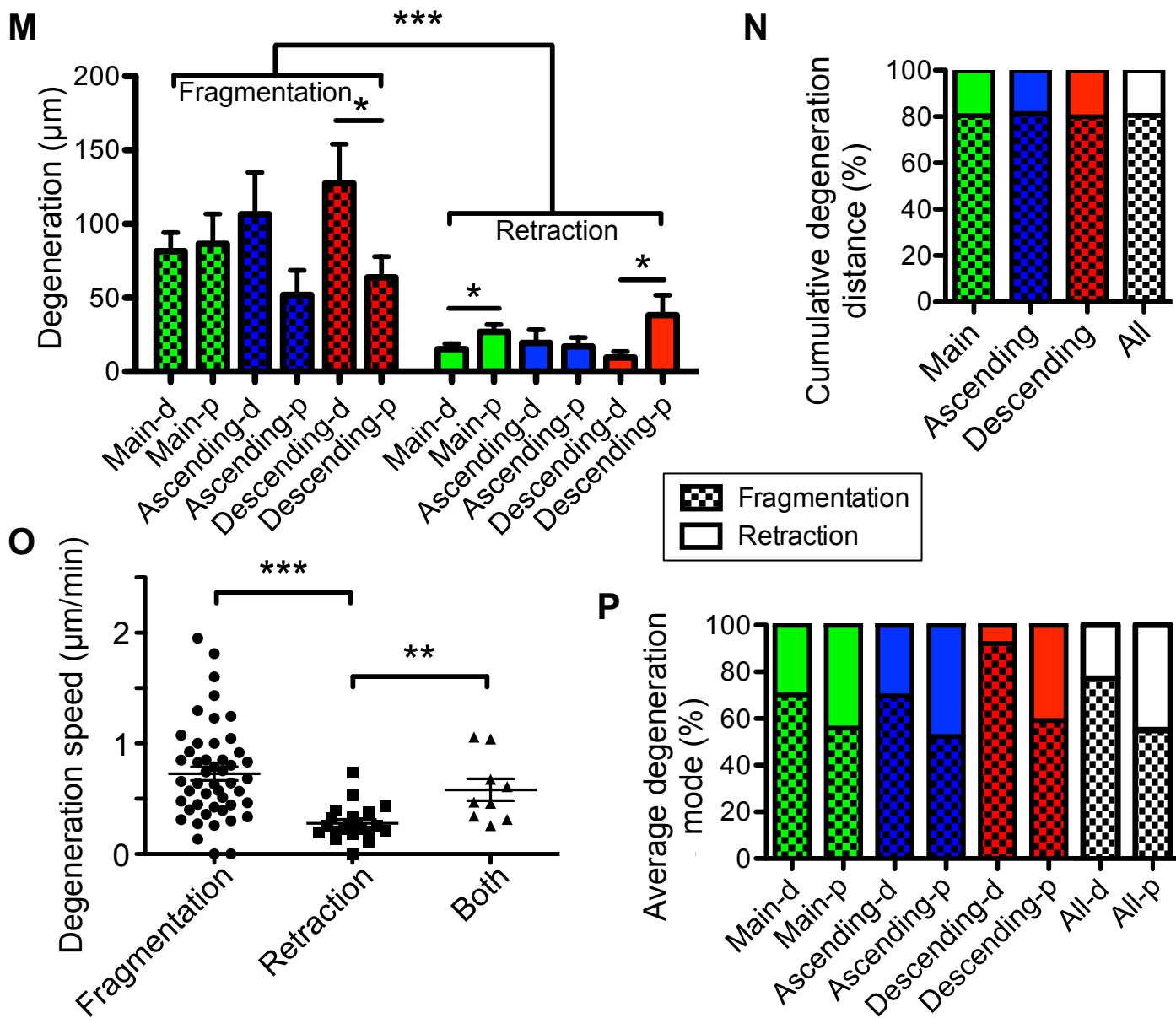


Figure S2



**Figure S2**  
**(Continued)**

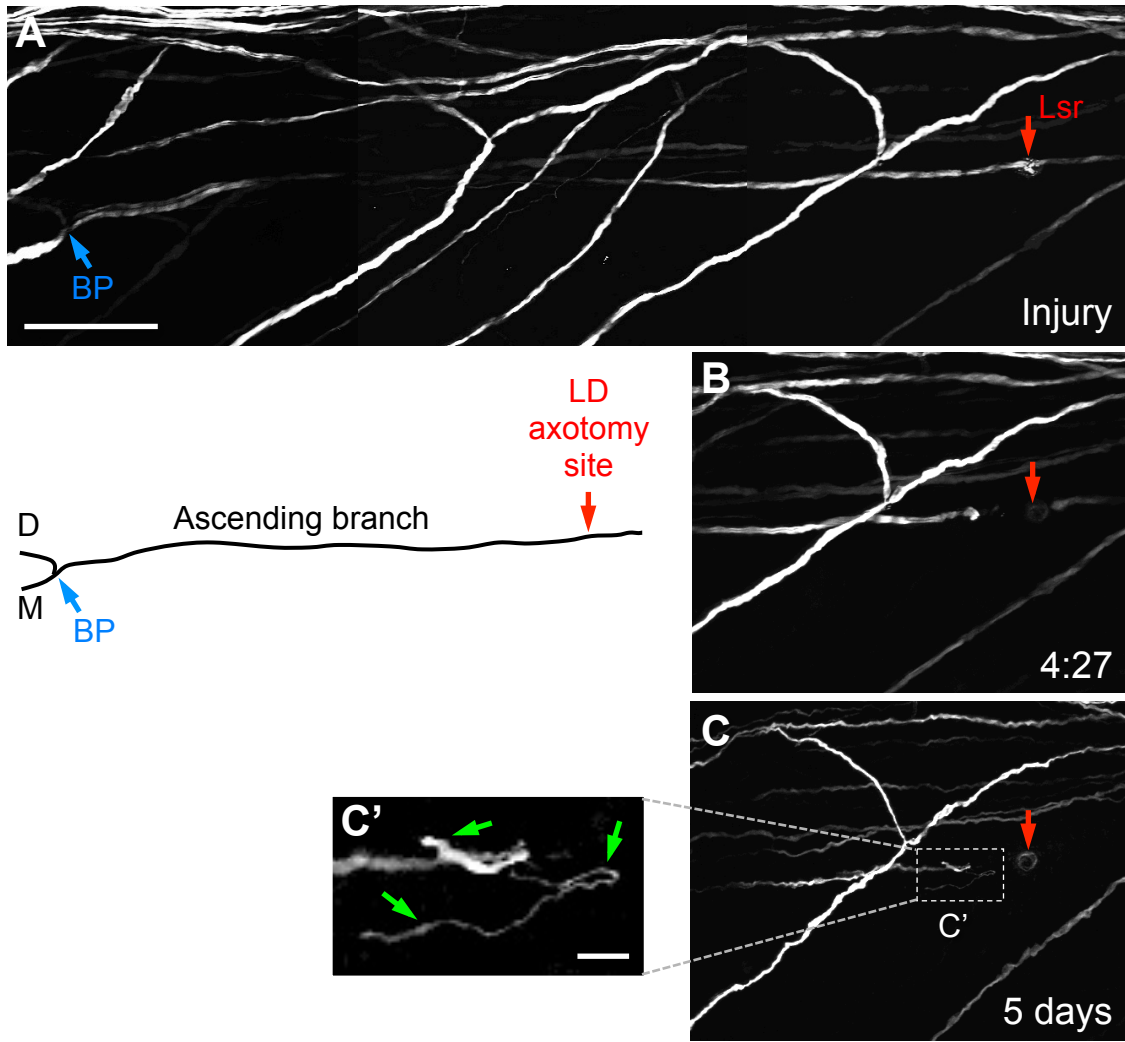
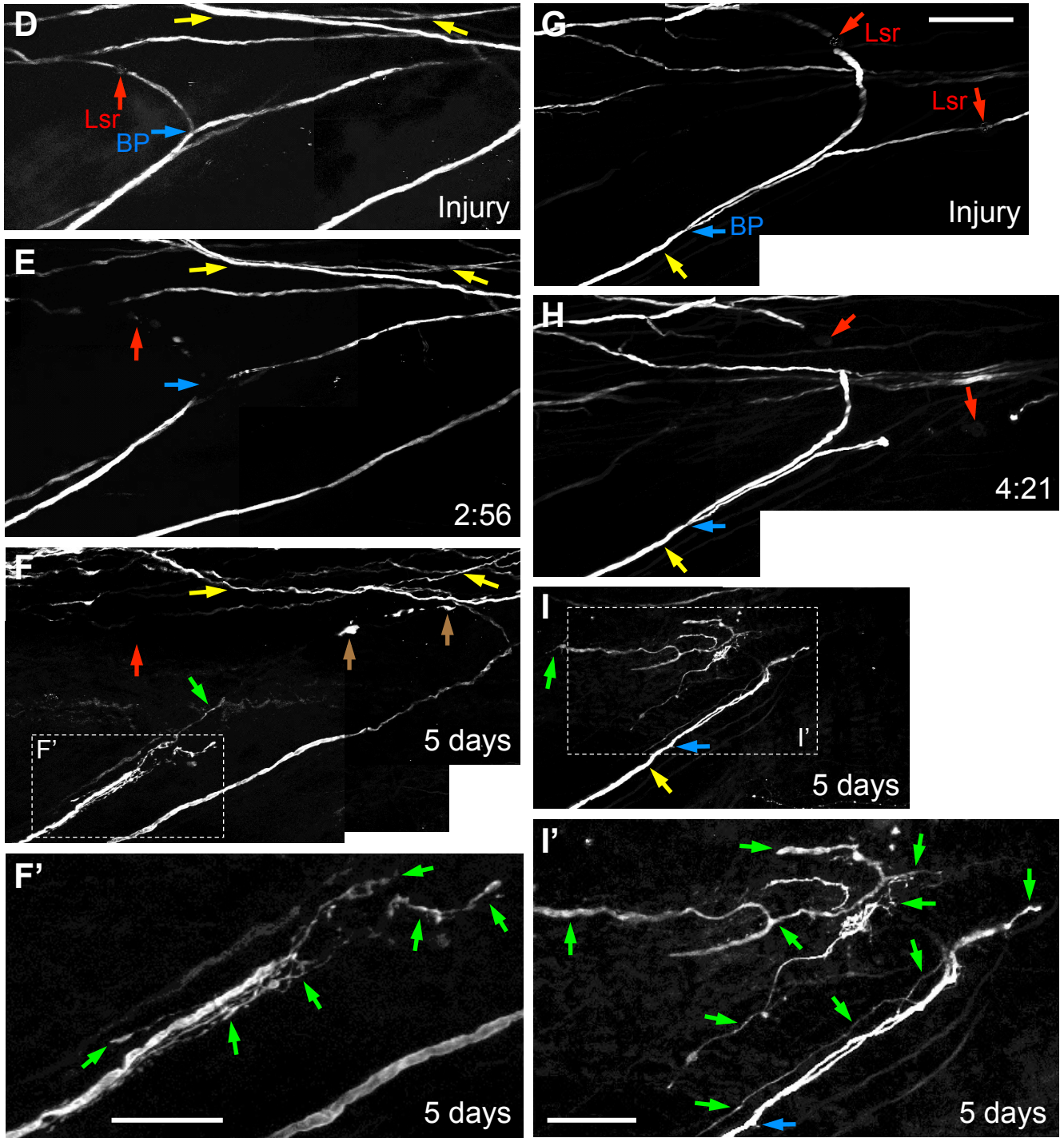


Figure S3



**Figure S3**  
**(Continued)**

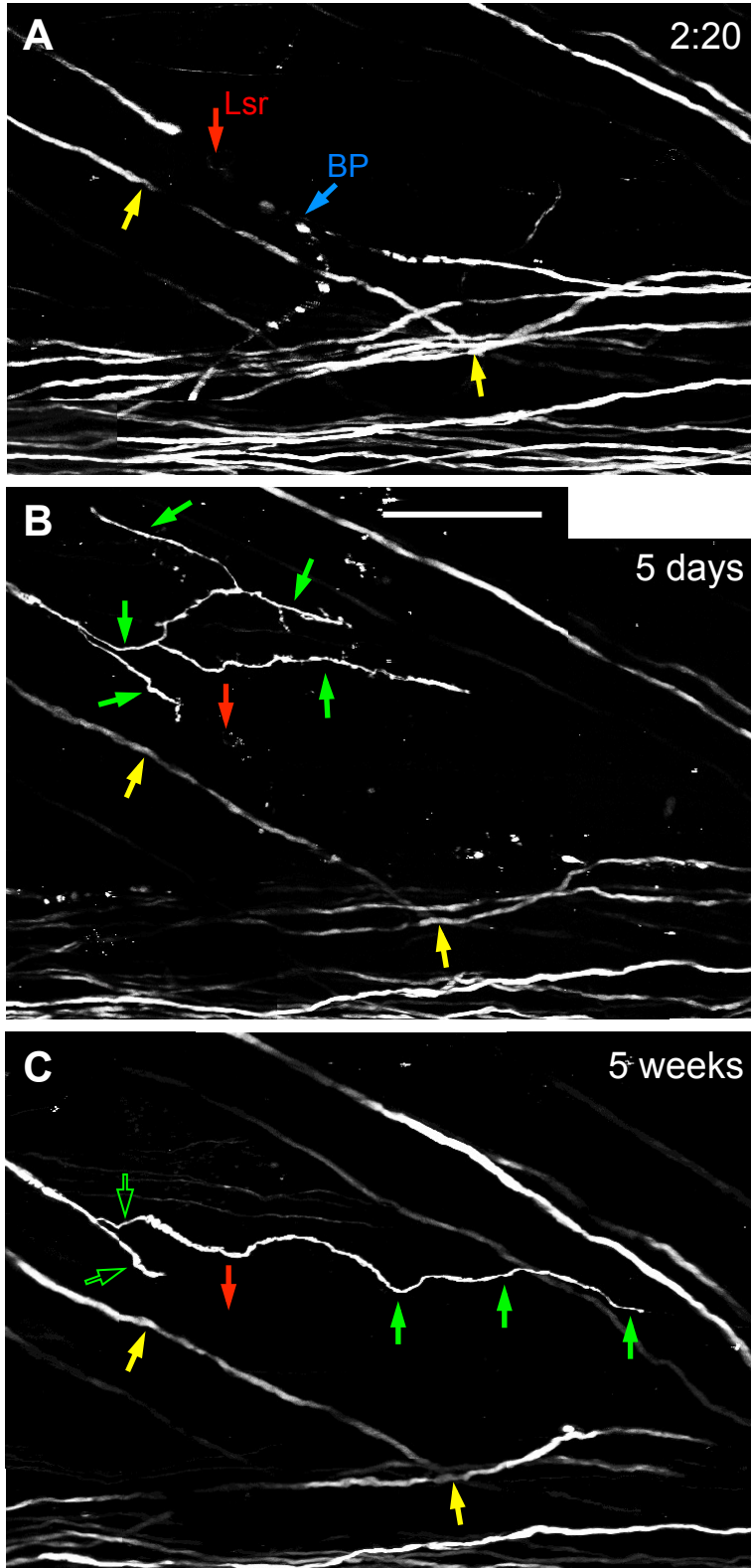


Figure S4

## SUPPLEMENTAL FIGURE LEGENDS

**Figure S1. Illustration of the in vivo imaging model** (related to Figure 1). (A) The axons to be imaged. A transverse section of the spinal cord at the mid thoracic level from an adult Thy1-YFP-H mouse is shown. Green, YFP labeled axons, most of which course along the rostral – caudal axis (perpendicular to the plane of section) in the white matter. Red, 5-HT (5-hydroxytryptamine, or serotonin) immunoreactivity as a counterstain to outline the grey matter. Dotted box outlines the area where the superficially located dorsal column sensory axons to be imaged in vivo reside. Note that many axonal populations are labeled by YFP, including a subset of the corticospinal axons (the two densely labeled, medially located axonal bundles just below the dorsal column sensory axons). (B) Schematic of the axotomy sites. BP, branch point (blue arrow); DRG, dorsal root ganglion; CNS, central nervous system; PNS, peripheral nervous system; wm, white matter; gm, grey matter. Solid green circle indicates sensory neuron cell body. Red crosses mark sites of axotomy: A, ascending branch; D, descending branch; M, main branch; LD, Long Distance (of ascending branch); Db, double axotomies of ascending and descending branches; p (lower case), proximal end or axonal segment; d (lower case), distal end or axonal segment. A, D, M, Db axotomies: ~100-150  $\mu\text{m}$  from the branch point (unless noted otherwise); LD axotomies: ~500-900  $\mu\text{m}$  (average ~700  $\mu\text{m}$ ) from the branch point. Along the spinal cord, dorsal column sensory axons send out collaterals that innervate the grey matter; the ascending branch ultimately makes synapses in the dorsal column nuclei of the brain stem; (not shown here). (C) The most dorsal part of a transverse Thy1-YFP-H spinal cord section stained for GFAP (blue) and P0 (red) to delineate the CNS – PNS boundaries (white arrows). DR, dorsal root. Note that the axons to be imaged (green, YFP direct fluorescence) are well within the CNS (area indicated by the dotted box). (D) A lower magnification dorsal view of the spinal cord to serve as a road map for higher magnification two-photon imaging. Axons enter the main bundle while bifurcating into an ascending branch and a descending branch. The boxed area was imaged with 2-photon microscopy shown in Figure 1A. Blood vessels appear as dark shadows (note the big dorsal vein in the middle of the cord and many fine vessels extending from it). Rostral is to the right in this and all other images. Scale bars = 200  $\mu\text{m}$  (A); 200  $\mu\text{m}$  (C); 200  $\mu\text{m}$  (D).

**Figure S2. Acute axon degeneration via fragmentation and retraction following laser axotomy** (related to Figure 1). (A-C) Example of an ascending branch axotomy where both the proximal and distal segments degenerated primarily via blebbing/fragmentation following axotomy. Note the small gap in axon immediately after axotomy (A), blebbing (B) and fragmentation (C). Branch points are usually bifurcation points; a white arrow in (A) indicates an example of a trifurcation point. (D-F) Example of an ascending branch axotomy where both the proximal and distal segments degenerated primarily via retraction. Note the small gap in axon immediately after axotomy (D) and continuous expansion of the gap in the absence of visible axonal fragments (E, F). Times shown are in hours and minutes (h:mm) after axotomy; “Injury” is the time point immediately after axotomy. (G-I) Degeneration following a descending branch axotomy, where the distal segment degenerated primarily via fragmentation while the proximal segment degenerated primarily via retraction. (J-L) Degeneration following a main branch axotomy, where the proximal segment degenerated primarily via fragmentation while the distal segment degenerated primarily via retraction. Lsr, laser axotomy; BP, branch point. Scale bar = 100  $\mu\text{m}$  (A-F); 100  $\mu\text{m}$  (G-L). (M) Average degeneration distances for

fragmentation and retraction at different injury locations at 2.5 hours after axotomy. d, distal; p, proximal.  $*p < 0.05$ , 2-tailed paired *t*-test.  $***p = 0.0001$ , 2-way ANOVA. Error bars = SEM. The average distance of fragmentation per axonal segment ( $85 \pm 13 \mu\text{m}$ ) was significantly larger than that of retraction ( $21 \pm 5.8 \mu\text{m}$ .  $p < 0.0001$ , Student's *t*-test,  $n = 78$  axonal segments, not shown on graph). (N) Fragmentation is the dominant degeneration mode across all injury locations. The percentage of cumulative degeneration distance from all axonal segments examined for fragmentation vs. retraction at 2.5 hour after axotomy is plotted. Cumulatively, fragmentation represented  $\sim 80\%$  of the distance degenerated, while retraction represented only  $\sim 20\%$ , regardless of the injury location. There was significantly more fragmentation than retraction.  $p < 0.01$ , 2-way ANOVA. (O) Degeneration speed differs between different degeneration modes. Axonal segments degenerating primarily via fragmentation ( $\geq 80\%$  distance degenerated), primarily via retraction ( $\geq 80\%$  distance) and via a combination of both ( $>20\%$  but  $<80\%$ ) are grouped separately (with the average degeneration speed of  $0.73 \pm 0.06$ ,  $0.28 \pm 0.03$  and  $0.58 \pm 0.10 \mu\text{m}/\text{min}$  respectively). About 67% of the fragmentation group had an average degeneration speed of  $\geq 0.5 \mu\text{m}/\text{min}$ , while only  $\sim 9\%$  of the retracting group did. Data are from 0-2.5 hours after axotomy.  $***p = 0.0001$ , and  $**p = 0.002$ , 2-tailed paired *t*-test. (P) The average percentage of degeneration mode is plotted for each group. Note that following axotomy, distal segments tend to fragment more and consequently retract less when compared with the proximal segments, regardless of the injury location.

**Figure S3. Examples of a Long Distance ascending branch axotomy, a descending branch axotomy leading to branch point breach and a double branch axotomy** (related to Figure 3). (A-C') An example of Long Distance ( $\sim 700 \mu\text{m}$  to the branch point) axotomy of an ascending branch when one could see the extent of retrograde degeneration on Day 0 (at 4h27m) and regeneration on Day 5 after axotomy. (D-F') A rare example of retrograde degeneration after a descending branch axotomy that breached the branch point, followed by axon regeneration observed at the subacute time point. (G-I') An example of double branch axotomy (of both ascending and descending branches) that led to axon regeneration. Scale bar =  $100 \mu\text{m}$  (A-C);  $10 \mu\text{m}$  (C');  $100 \mu\text{m}$  (D-F);  $50 \mu\text{m}$  (F'),  $100 \mu\text{m}$  (G-I);  $50 \mu\text{m}$  (I'). Red arrow, laser axotomy (Lsr); blue arrow, branch point (BP); yellow arrows, landmarks; green arrows, newly regenerated axons; brown arrows, Wallerian degeneration.

**Figure S4. Dynamic regeneration, pruning and remodeling** (related to Figure 4). An example of a main branch axotomy that was imaged up to the subchronic time point. Note that multiple new branches at Day 5 were later pruned but one branch survived and extended further by 5 weeks after axotomy. Red arrow, laser axotomy; yellow arrows, landmarks; solid green arrows, new axonal regeneration; hollow green arrows, previous axon regeneration that sustained at 5 weeks. Scale bar =  $100 \mu\text{m}$ .

## SUPPLEMENTAL MOVIE

**Movie S1. An example of time-lapse imaging of acute axon degeneration following a main branch axotomy with 2-photon microscopy** (related to Figure 1). The axon depicted here is the same as shown in Fig. 1A-J, but showing more frequent sampling. Red arrow marks laser axotomy site. Times shown are hours and minutes (h:mm). Scale bar =  $100 \mu\text{m}$ .

## **SUPPLEMENTAL EXPERIMENTAL PROCEDURES**

### **Animal surgeries**

Adult Thy1-YFP-H transgenic mice (Feng et al., 2000), backcrossed to C57BL/6 for a minimum of 10 generations ( $\geq N10$ ) and 8-12 weeks old, were used for this study. All procedures in this study were approved by the Institutional Animal Care and Use Committee at UCSD. Our imaging paradigm allows for stable and repetitive imaging of spinal axons without disrupting dura or the need for intubation as we described previously (Davalos et al., 2008). For surgical procedures, mice were anaesthetized with 100 mg/kg ketamine (Fort Dodge Animal Health, Fort Dodge, IA), 15 mg/kg xylazine (Vedco, Saint Joseph, MO) and 2.5 mg/kg acepromazine (Vedco, Saint Joseph, MO) in a 0.9% NaCl solution, as described (Davalos et al., 2008). Supplemental anesthesia was provided at half the dosage when necessary. This anesthetic cocktail minimizes breathing-associated movement artifacts. The midline of the back was shaved and sterilized with 70% ethanol. A midline dermal incision (~1 cm in length) was made to expose the vertebral muscles. The vertebral muscles were carefully removed to expose the thoracic vertebrae at the T8-T10 level and a laminectomy at the T9 level of the spinal cord was made to expose the spinal cord.

The spinal column was stabilized with customized Narishige spinal cord clamps and head holding adaptors mounted on a steel plate. The clamps were placed on both the T8 and T10 vertebrae to stabilize the spinal column, while the head was placed in the head holding adaptor, and the tail was clamped so that the mouse maintained a relatively level position. A well of petroleum jelly was created around the exposed spinal cord and filled with artificial cerebrospinal fluid (ACSF) in order to allow for the preservation of the cord and the immersion of the objective lens.

After the imaging session was completed, the wound was closed and skin sutured. Animals were allowed to recover on a heating pad and given 0.05 mg/kg buprenorphine subcutaneously every 12 hours for 5 days, sterile saline for dehydration, and Baytril. For terminal procedures, animals were overdosed with 10 mg/kg of Nembutal (Ovation Pharmaceuticals, Deerfield, IL).

### **In vivo imaging of ascending spinal sensory axons**

After the mouse was secured in the stabilization device, it was then placed in a heat-controlled chamber underneath a customized FV300 Olympus microscope as described (Davalos and Akassoglou, 2012; Davalos et al., 2008). Imaging was performed with a Spectra Physics Mai-Tai laser tuned to 920 nm for two-photon excitation of YFP. First, an Olympus 10x 0.3 NA water-immersion lens was used to obtain an image of the entire imaging area to serve as a roadmap (as in Fig. S1D). From this dorsal overview, sensory axons labeled with YFP can be seen entering the spinal cord and bifurcating into an ascending and a descending branch. Occasionally an axon trifurcates (as in Fig. S2A, white arrow). For 2-photon imaging, an Olympus 40x 0.8 NA water-immersion lens was used. Axons were chosen for imaging based on the visibility of the axon, proximity to the branch point and ease of identification of nearby landmarks (e.g. distinct morphologies of other surrounding axons, in an area that is not too densely or too sparsely populated by fluorescently labeled axons).

For laser axotomy, we used the point function in the Spectra Physics Mai Tai Software for the Ti:Sapphire laser, with a duration of 0.2 second without a neutral density filter at a wavelength of 820 nm. The average power output was 1-1.5 Watts for each laser axotomy

event. This allowed us to focally sever a single labeled axon without visible damage to adjacent labeled axons. When the initial laser “cut” was visibly complete, in no instance did reconnection of the proximal and distal segments occur, indicating that reconnection that has been reported in *C. elegans* (Ghosh-Roy et al., 2010; Neumann et al., 2011) is either nonexistent or exceedingly rare. We initially chose to axotomize the ascending, descending or main branch close (~100-150  $\mu\text{m}$ ) to the branch point for ease of tracking the axotomy site (Fig. S1B). The ascending branch travels up the spinal cord, eventually terminating in the *nucleus gracilis*. The descending branch initially projects down the cord and then innervates the spinal grey matter. The main branch is part of the axon before it bifurcates in the spinal cord. Once axotomized, the part of the axon that is closer (and still connected) to the cell body is the proximal segment, and the part that is further away (and disconnected) from the cell body is the distal segment.

After laser ablation, the axon was imaged for up to ~5 hours to capture the acute axonal degeneration. In a typical experiment, we stopped the first imaging session on Day 0 after acute degeneration had subsided. For re-imaging experiments on a later day, animals were anesthetized as described above, the original wound was reopened, and any tissue overgrowth on top of the spinal cord was removed to expose the original imaged area. With experience, the axon that was axotomized and imaged previously could be definitively identified by the morphology of the axon and nearby landmarks. In this regard, the low-resolution roadmap was particularly useful. Even though our imaging paradigm does not involve traumatic spinal cord injury, the surgical procedure itself still elicited some tissue responses, including the thickening of the local blood vessels (which appear as dark shadows in the images taken, as in Fig. S1D, dorsal vein) and changes in the morphology of the axons. Some of the changes in the appearance of axons were due to different angles of view between imaging sessions. Axons that could not be definitively identified as the previously axotomized and imaged axons were excluded from the analyses (representing about 10-15% of axons imaged initially). All animals included in the study had normal ambulation and did not exhibit any gross signs of motor dysfunction after each surgery. Animals that displayed motor deficits or any visible trauma to the spinal cord such as bruising after any surgery were excluded.

Acquisition of the images was executed with Olympus FluoView software. Z-stacks were taken every 10  $\mu\text{m}$  with the 10x objective (as roadmap), and every 1  $\mu\text{m}$  with the 40x objective (2-photon) throughout the entire focal area spanning 50 – 200  $\mu\text{m}$ . During acquisition, laser power and offset were adjusted to minimize background. The final images presented here are maximum intensity projections along the Z-axis. For image presentation, only brightness and contrast were manipulated using Adobe Photoshop.

### **Quantification and statistical analyses**

ImageJ was used to quantify axonal responses to axotomy. For both the proximal and distal segments, the distance of axon degeneration was measured from the center of the axotomy site to the closest tip of the remaining continuous axonal segment using the segmented line function. These quantifications were done in 2D, from the maximum projection Z-stack, as axon degeneration occurred almost exclusively along the rostral – caudal axis. We measured sub-acute regeneration as any new growth from the terminal tip of the injured axon. For more chronic time points, new growth was growth compared to the last time point observed, while net axon growth was the growth compared to the last observation time point on Day 0. For all sub-acute and chronic time points, we measured regeneration in 3D using the simple neurite

tracer plugin for Fiji, as regenerating axons often took a tortuous route and could travel for a significant distance along the dorsal – ventral and/or medial/lateral axis. Regeneration was only positively identified when there was at least 10  $\mu\text{m}$  of new growth.

One-way ANOVA was used for multiple comparisons with Bonferroni post-test. For multiple observations between groups we used two-way ANOVA. Unpaired *t*-tests were used for pairwise comparisons. Results are expressed as mean values  $\pm$  SEM. The chi-square test was used for group frequency data, and the Fisher's exact test was used to determine significance between specific groups. A *p* value of  $< 0.05$  was considered to be statistically significant. All statistical analyses were performed using GraphPad Prism.

### **Immunohistochemistry**

Mice were perfused transcardially with 4% paraformaldehyde (PFA) in phosphate-buffered saline (PBS). The spinal cord was carefully dissected so as to keep all dorsal root ganglia intact, post-fixed for 2 hours, cryoprotected in 30% sucrose with PBS overnight at 4°C. A segment of the thoracic cord (T8-10) was embedded in OCT (Sakura Fine Tech, Japan). Transverse sections were cut on a cryostat at 20  $\mu\text{m}$  and collected on Superfrost Plus slides (Fisher Scientific). Sections were washed in PBS, blocked for 90 minutes in 5% normal goat serum (NGS) (Vector Labs) with PBS, and incubated overnight at 4° with antibodies: 1:100 anti-P0 (Abcam), and 1:500 anti-GFAP (Dako). Sections were rinsed in PBS and incubated with secondary antibodies (1:500 goat anti-rabbit Alexa 350 and 1:500 goat anti-chicken Alexa 546) (Invitrogen) in 5% NGS for 90 minutes. Sections were rinsed in PBS and coverslipped with Fluoromount-G (Southern Biotech). Images were captured and analyzed with an Axio Imager fluorescent microscope (Zeiss).

### **Supplemental References**

Davalos, D., and Akassoglou, K. (2012). In vivo imaging of the mouse spinal cord using two-photon microscopy. *Journal of visualized experiments : JoVE*, e2760.

Davalos, D., Lee, J.K., Smith, W.B., Brinkman, B., Ellisman, M.H., Zheng, B., and Akassoglou, K. (2008). Stable in vivo imaging of densely populated glia, axons and blood vessels in the mouse spinal cord using two-photon microscopy. *J Neurosci Methods* 169, 1-7.

Feng, G., Mellor, R.H., Bernstein, M., Keller-Peck, C., Nguyen, Q.T., Wallace, M., Nerbonne, J.M., Lichtman, J.W., and Sanes, J.R. (2000). Imaging neuronal subsets in transgenic mice expressing multiple spectral variants of GFP. *Neuron* 28, 41-51.

Ghosh-Roy, A., Wu, Z., Goncharov, A., Jin, Y., and Chisholm, A.D. (2010). Calcium and cyclic AMP promote axonal regeneration in *Caenorhabditis elegans* and require DLK-1 kinase. *J Neurosci* 30, 3175-3183.

Neumann, B., Nguyen, K.C., Hall, D.H., Ben-Yakar, A., and Hilliard, M.A. (2011). Axonal regeneration proceeds through specific axonal fusion in transected *C. elegans* neurons. *Dev Dyn* 240, 1365-1372.